nature
neuroscience

Competitive regulation of synaptic Ca^{2+} influx by D2 dopamine and A2A adenosine receptors

Michael J Higley[1,2] & Bernardo L Sabatini[1]

Striatal D2-type dopamine receptors (D2Rs) have been implicated in the pathophysiology of neuropsychiatric disorders, including Parkinson's disease and schizophrenia. Although these receptors regulate striatal synaptic plasticity, the mechanisms underlying dopaminergic modulation of glutamatergic synapses are unclear. We combined optogenetics, two-photon microscopy and glutamate uncaging to examine D2R-dependent modulation of glutamatergic synaptic transmission in mouse striatopallidal neurons. We found that D2R activation reduces corticostriatal glutamate release and attenuates both synaptic- and action potential–evoked Ca^{2+} influx into dendritic spines by approximately 50%. Modulation of Ca^{2+} signaling was mediated by a protein kinase A (PKA)-dependent regulation of Ca^{2+} entry through NMDA-type glutamate receptors that was inhibited by D2Rs and enhanced by activation of 2A-type adenosine receptors (A2ARs). D2Rs also produced a PKA- and A2AR-independent reduction in Ca^{2+} influx through R-type voltage-gated Ca^{2+} channels. These findings reveal that dopamine regulates spine Ca^{2+} by multiple pathways and that competitive modulation of PKA controls NMDAR-mediated Ca^{2+} signaling in the striatum.

The striatum is the first processing stage in the basal ganglia, a collection of forebrain nuclei whose function is critical for the generation of coordinated, purposeful movements[1]. Regulation of striatal activity by dopamine is important for a variety of psychomotor functions, including habit learning and serial movement, and perturbation of dopaminergic signaling is central to the pathogenesis of several neuropsychiatric diseases[2–4]. Dopamine release in the striatum activates two classes of G protein–coupled receptors that are expressed by distinct subpopulations of medium spiny neurons (MSNs), the principal striatal cells. D2Rs, expressed by striatopallidal MSNs, are linked to behavioral disorders, including Parkinson's disease, obsessive-compulsive disorder and schizophrenia[2,4,5]. D2Rs are coupled to $G\alpha_i$[2,3,6], whose activation triggers a divergent cascade of signaling pathways, reducing cAMP production and PKA activity while simultaneously enhancing phospholipase C (PLC)-dependent processes and the release of Ca^{2+} from internal stores[3,4,6]. Striatopallidal MSNs also express the $G\alpha_s$-coupled A2AR, whose activation elevates cAMP and PKA activity and may counteract the actions of D2Rs[7]. Nevertheless, the cellular targets of dopaminergic and adenosinergic signaling are not well characterized.

The expression of D2Rs on dendritic shafts and spines, as well as on afferent glutamatergic terminals, suggests that an important feature of D2R-mediated modulation may be the control of excitatory synaptic transmission[8]. Activation of D2Rs has been reported to inhibit postsynaptic glutamate receptors stimulated by exogenous agonists[9] and to reduce glutamate release, although it remains unclear whether this effect is mediated by pre- or postsynaptic D2Rs[10,11]. D2R activation also reduces whole-cell Ca^{2+} influx through voltage-gated Ca^{2+} channels (VGCCs)[12–14], although the consequences for synaptic Ca^{2+}

influx are unknown. Indeed, recent work suggests that D2Rs might indirectly boost synaptic Ca^{2+} influx by decreasing acetylcholine release from local interneurons, relieving cholinergic inhibition of dendritic VGCCs[15]. Functionally, D2R activation promotes long-term depression (LTD) of striatal excitatory synapses while reducing NMDA-type glutamate receptor (NMDAR)-dependent long-term potentiation (LTP)[16–19]. The former is thought to rely on a D2R-mediated, PLC-dependent enhancement of endocannabinoid release[20,21], whereas the mechanisms underlying the latter are unknown.

To gain insight into D2R actions during synaptic transmission, we combined electrophysiological recordings and two-photon imaging of striatopallidal MSNs with optical activation of glutamatergic synapses using channelrhodopsin-2 (ChR2) and focal glutamate uncaging. We found that D2Rs reduced corticostriatal glutamatergic transmission without directly altering current through postsynaptic glutamate receptors. Instead, D2R activation selectively inhibited Ca^{2+} influx through both NMDARs and R-type VGCCs. Regulation of NMDARs was mediated by a PKA-dependent pathway and could be prevented by coactivation of A2ARs. In contrast, modulation of R-type Ca^{2+} influx was independent of PKA and A2AR activity. Our findings indicate that D2Rs engage a divergent signaling cascade controlling synaptic Ca^{2+} influx and suggest that A2ARs and D2Rs compete to regulate Ca^{2+} influx through NMDARs.

RESULTS

To investigate D2R actions on glutamatergic responses in striatopallidal MSNs, we made whole-cell current-clamp recordings from green fluorescent protein (GFP)-positive cells in acute slices prepared from mice expressing GFP under control of the *Drd2* gene promoter (**Fig. 1a**)[15,22].

[1]Howard Hughes Medical Institute, Department of Neurobiology, Harvard Medical School, Boston, Massachusetts, USA. [2]Present address: Department of Neurobiology, Program in Cellular Neuroscience, Neurodegeneration, and Repair, Yale School of Medicine, New Haven, Connecticut, USA. Correspondence should be addressed to B.L.S. (bsabatini@hms.harvard.edu).
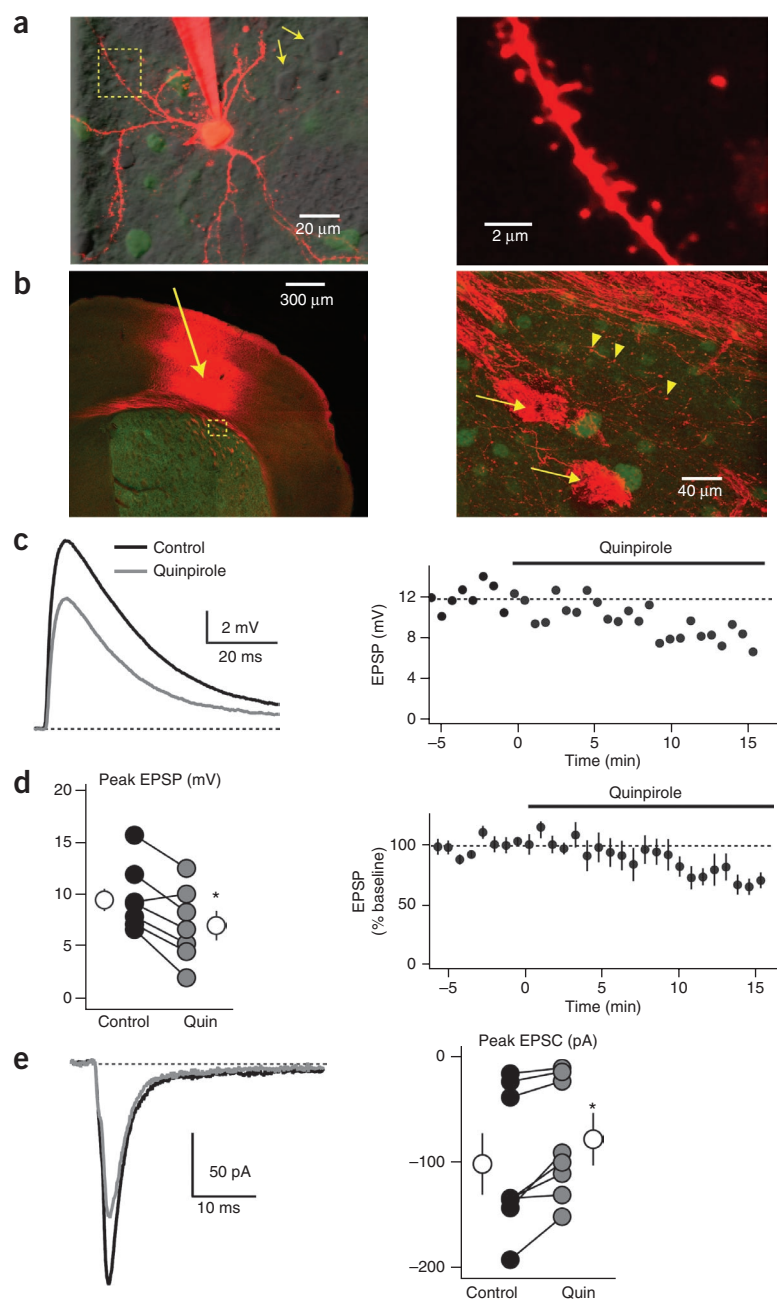
Figure 1 Modulation of corticostriatal synaptic responses in striatopallidal MSNs by D2Rs. (**a**) Left, two-photon laser-scanning microscopy image of a GFP-positive D2R-expressing striatopallidal MSN filled with the red fluorophore Alexa Fluor 594 through the recording pipette. Nearby nonrecorded GFP-positive cells are also visible. GFP-negative, putatively D2R-negative MSNs are shown by simultaneous laser-scanning differential interference contrast (yellow arrows). Right, higher magnification image of the region bounded by the yellow box on the left. Spines are visible along the dendritic branch. (**b**) Left, confocal image of a coronal section from the striatum of an Emx1-Cre/Drd2-GFP mouse. Green fluorescence indicates GFP expression in D2R-expressing MSNs. Red fluorescence indicates the presence of the Channelrhodopsin-mCherry fusion protein in corticostriatal cells and axons. Arrow indicates site of adenoassociated virus injection, 10 d prior. Right, higher magnification image of the region bounded by the yellow box on the left. Arrows indicate large bundles of descending corticobulbar fibers passing through the striatum. Arrowheads indicate presumed presynaptic varicosities of axonal branches arborizing in the striatum. (**c**) Left, light-evoked EPSPs recorded from a striatopallidal MSN in control conditions and after wash-in of 8 μM quinpirole. EPSPs are averages of five consecutive trials. Right, time course of the evoked EPSP amplitude from the experiment shown on the left. Quinpirole was applied during the time indicated by the horizontal bar. (**d**) Left, peak values for light-evoked EPSPs for each recorded cell ($n = 7$, closed circles) in control conditions (black) and after quinpirole wash-in (gray). The average population data are also shown (open circles). Right, average ($n = 7$) time course of the evoked EPSP amplitude for the cells shown on the left. Quinpirole was applied during the time indicated by the horizontal bar. (**e**) Left, light-evoked EPSCs recorded from a striatopallidal MSN in control conditions and after wash-in of 8 μM quinpirole. EPSCs are averages of five consecutive trials. Right, peak values for light-evoked EPSCs for each recorded cell ($n = 8$, closed circles) in control conditions (black) and after quinpirole wash-in (gray). The average population data are also shown (open circles). *$P < 0.05$.

Membrane potential was held near −60 mV, and experiments were carried out in the presence of the muscarinic antagonist scopolamine.

To examine modulation of corticostriatal synapses, we expressed ChR2 in motor cortex neurons projecting to the striatum (**Fig. 1b**, Online Methods). Pulses of blue light applied to the striatum surrounding the current-clamped MSN reliably evoked excitatory postsynaptic potentials (EPSPs; **Fig. 1c**). Bath application of the D2R agonist quinpirole reduced the average EPSP amplitude from 9.6 ± 1.2 mV to 7.0 ± 1.4 mV ($n = 7$, Student's paired t test, $P < 0.01$; **Fig. 1d**). In voltage-clamp recordings, application of quinpirole reduced light-evoked excitatory postsynaptic currents (EPSCs) from 101.4 ± 23.2 pA to 78.6 ± 19.4 pA ($n = 8$, $P < 0.01$; **Fig. 1e**). Notably, quinpirole failed to alter EPSPs evoked by local electrical stimulation (**Supplementary Fig. 1**), suggesting that electrical stimulation may trigger local release of dopamine, occluding the actions of exogenous agonists[11].

Previous studies found that D2R activation reduces glutamate release from corticostriatal terminals[10,11], potentially explaining the inhibition of light-evoked EPSPs and EPSCs. Evidence for direct D2R modulation of postsynaptic glutamate receptors has been less conclusive. We combined two-photon laser-scanning microscopy and glutamate uncaging to bypass presynaptic terminals and examine modulation of glutamatergic responses at single postsynaptic sites. Cells were filled with the Ca^{2+}-insensitive red fluorophore Alexa Fluor 594 and the Ca^{2+}-sensitive green fluorophore Fluo-5F. Under current clamp, a 500-μs pulse from the uncaging laser directed 0.5 μm from a dendritic spine located within 60 μm of the cell body produced a small uncaging-evoked EPSP (uEPSP) and a Ca^{2+}-dependent increase in green fluorescence in the spine head and neighboring dendritic shaft (**Fig. 2a**). Fluorescence transients in the spine and dendrite were quantified as the percent increase in green signal relative to
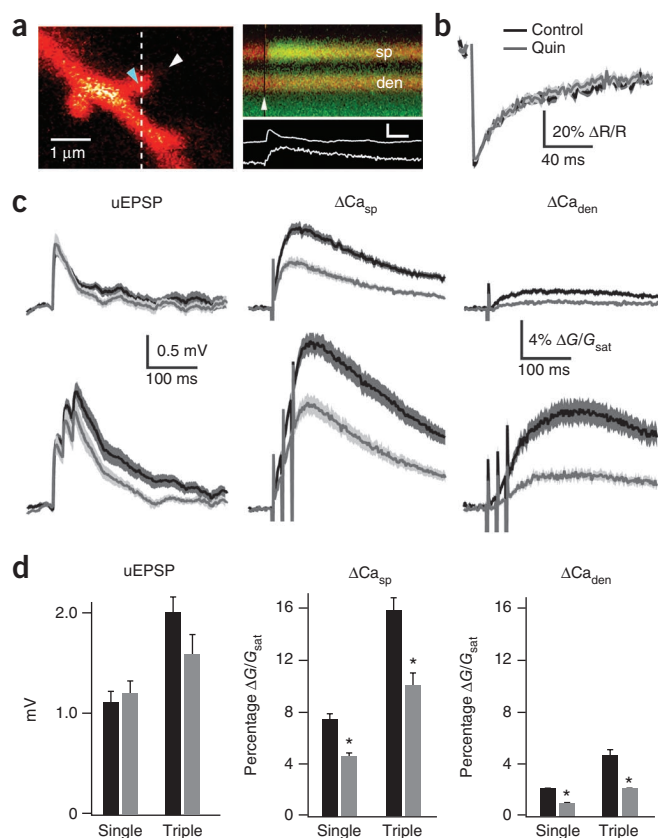
Figure 2 D2R modulation of uncaging-evoked Ca^{2+} transients in active spines. (**a**) Left, two-photon laser-scanning microscopy image of a spiny region from a striatopallidal MSN dendrite filled with the red fluorophore Alexa Fluor 594 and the green Ca^{2+}-sensitive indicator Fluo 5F. Right, red and green fluorescence in the spine head (sp) and neighboring dendrite (den) measured in line scan over the region indicated by the dashed line on the left. The white arrowheads on the left and right indicate the location and timing, respectively, of a 500-µs pulse of 725-nm laser light used to focally uncage glutamate near the spine head. The increase in green fluorescence indicates increased intracellular Ca^{2+}. Background green fluorescence visible at the bottom of the image is a result of GFP in an adjacent unrecorded MSN. The corresponding uEPSP and spine Ca^{2+} transient (white traces) are shown below. Inset scale bars represent 1 mV, 5% $\Delta G/G_{sat}$, 50 ms. (**b**) Recovery of red fluorescence following photobleaching was used to set laser power. The uncaging laser was directed to the spot indicated by the blue arrowhead in **a** and red fluorescence was measured in line scan from the region indicated in **a**. Power was adjusted such that a 500-µs pulse produced ~50% reduction in red fluorescence. Average photobleaching transients are shown for control conditions (black, $n = 36$) and in the presence of quinpirole (gray, $n = 23$). Solid lines indicate the mean and the shaded regions indicate the mean ± s.e.m. (**c**) Uncaging-evoked uEPSPs (left), ΔCa_{sp} (middle) and ΔCa_{den} (right) produced by single (upper traces) or 50-Hz triple (lower traces) uncaging stimuli are shown for control conditions (black) and in the presence of quinpirole (gray). Mean (solid lines) and mean ± s.e.m. (shaded regions) are shown. (**d**) Population data for peak uEPSP (left), ΔCa_{sp} (middle) and ΔCa_{den} (right) evoked by single or triple uncaging stimuli in control conditions (black) and in the presence of quinpirole (gray) are shown. *$P < 0.05$.

the maximal green fluorescence in saturating Ca^{2+} ($\Delta G_{sp}/G_{sat}$ and $\Delta G_{den}/G_{sat}$, respectively; see Online Methods). For each synapse, laser power was adjusted such that the uncaging pulse applied directly to the spine head bleached ~50% of the red fluorescence (**Fig. 2b**)[23], and the periphery of the spine head was probed to find the uncaging position that evoked the largest uEPSP[24].

Under control conditions, a single uncaging pulse produced an average ($n = 36$) uEPSP and associated Ca^{2+} transients in the spine and neighboring dendritic shaft with amplitudes of 1.1 ± 0.1 mV, 7.4 ± 0.5% and 1.9 ± 0.2%, respectively (**Fig. 2c,d**). Because MSN dendrites exhibit voltage-dependent conductances that can shape temporal integration of synaptic inputs[25,26], we also measured the average uEPSP (2.0 ± 0.2 mV) and Ca^{2+} transients ($\Delta G_{sp}/G_{sat}$ = 15.8 ± 1.1%, $\Delta G_{den}/G_{sat}$ = 4.7 ± 0.2%) evoked by a burst of uncaging pulses (three stimuli, 20-ms interstimulus interval; **Fig. 2c,d**). In the presence of quinpirole ($n = 23$), there was no significant change in average peak uEPSP magnitude for either single (1.2 ± 0.1 mV, $P = 0.61$) or triple (1.6 ± 0.2 mV, $P = 0.14$) stimuli (**Fig. 2c,d**) compared with control conditions, although the decay of the triple response was slightly faster, possibly indicating changes in voltage-gated ion channel or NMDAR contributions. In contrast, quinpirole strongly reduced uncaging-evoked Ca^{2+} influx following both single ($\Delta G_{sp}/G_{sat}$ = 4.2 ± 0.4%, $P < 0.0001$; $\Delta G_{den}/G_{sat}$ = 0.9 ± 0.1%, $P < 0.0001$) and triple ($\Delta G_{sp}/G_{sat}$ = 9.4 ± 0.8%, $P < 0.0001$; $\Delta G_{den}/G_{sat}$ = 1.9 ± 0.2%, $P < 0.001$) stimuli (**Fig. 2c,d**). Quinpirole did not alter the kinetics of recovery following photobleaching of the red fluorophore (50.7 ± 5.2 ms versus 58.6 ± 10.4 ms for control and quinpirole, respectively, $P = 0.45$; **Fig. 2b**), indicating a lack of change in the diffusional properties of the spine. Furthermore, temporal summations of uEPSPs and Ca^{2+} transients were not significantly altered by quinpirole ($P > 0.05$ for all comparisons; **Supplementary Fig. 2**). In summary, when bypassing the presynaptic

terminal, activation of D2Rs in striatopallidal MSNs reduced synaptic Ca^{2+} influx by nearly 50% with minimal effects on somatic potentials.

Multiple sources contribute to synaptic Ca^{2+} transients

To identify potential targets of dopaminergic regulation underlying the inhibition of Ca^{2+} influx, we examined the Ca^{2+} sources that contribute to synaptic signaling in striatopallidal MSNs. Blockade of NMDARs with the selective antagonist 3-(2-carboxypiperazin-4-yl)propyl-1-phosphonic acid (CPP) significantly increased the average ($n = 21$) amplitude of the single stimulus uEPSP to 146.3 ± 20.7% of the control value ($P < 0.05$; **Fig. 3**). This counterintuitive result may reflect the role of NMDARs in promoting the opening of SK-type Ca^{2+}-activated potassium channels that inhibit synaptic potentials in a variety of cell types[23,27]. Indeed, application of the SK channel blocker apamin (0.1 µM) also significantly increased uEPSP amplitude ($P < 0.001$; **Supplementary Fig. 3**). A 50-Hz burst stimulus revealed that temporal summation was decreased by NMDAR blockade as a result of reduced uEPSP duration (**Fig. 3a** and **Supplementary Fig. 2**). CPP reduced the uncaging-evoked Ca^{2+} influx in the spine head to 14.0 ± 1.3% ($P < 0.0001$) and 9.1 ± 1.0% ($P < 0.0001$) of control values for single and triple stimuli, respectively (**Fig. 3**), consistent with a dominant contribution of NMDARs to synaptically evoked Ca^{2+} transients.

We also analyzed the contribution of VGCCs to synaptic signaling. Selective blockade of P/Q- ($n = 24$), N- ($n = 26$) or L-type ($n = 26$) channels (with 0.2 µM ω-agatoxin-IVA, 1 µM ω-conotoxin GVIA or 3 µM nimodipine, respectively) had no significant effect on synaptic potentials and Ca^{2+} transients evoked by single or triple stimuli ($P > 0.05$ for all comparisons; **Fig. 3b–d**). These blockers also failed to alter the temporal summation of uncaging-evoked potentials and Ca^{2+} transients (**Supplementary Fig. 2**). As shown previously[28], 20 µM nimodipine reduced Ca^{2+} influx (**Supplementary Fig. 4**), indicating that either channel selectivity decreases at this high concentration[29] or that relatively dihydropyridine-resistant Ca$_V$1.3 L-type channels are present[30].

Combined blockade of R-, L- and T-type channels with mibefradil had no effect on the average ($n = 18$) uEPSP evoked by a

Figure 3 Multiple Ca^{2+} sources contribute to synaptic Ca^{2+} signaling. (**a**) Uncaging-evoked uEPSPs (upper two traces) and associated ΔCa_{sp} (lower two traces) produced by single or triple (50 Hz) uncaging pulses are shown. Mean (black solid lines) and mean ± s.e.m. (shaded regions) are shown for responses evoked in the presence of the NMDAR antagonist CPP ($n = 21$). Light gray shaded regions indicate the mean ± s.e.m. responses under control conditions, reproduced from **Figure 2**. (**b**) Traces are arranged as in **a** for responses evoked in VGCC blockers, as indicated above each column: mibefradil (Mib, $n = 18$), SNX-482 (SNX, $n = 20$), ω-agatoxin IVA (Aga, $n = 24$), ω-conotoxin GVIA (GVIA, $n = 26$) and nimodipine (Nim, $n = 26$). Light gray shaded regions indicate the mean ± s.e.m. responses under control conditions. (**c**) Population data for peak uEPSP, expressed as a percentage of the control value, for each stimulus and condition shown in **a** and **b**. (**d**) Population data for ΔCa_{sp}, expressed as a percentage of the control value, for each stimulus and condition shown in **a** and **b**. *$P < 0.05$.

single stimulus, although the uEPSP following the triple stimulus was reduced relative to control (**Fig. 3b,c**). However, mibefradil reduced the average relative amplitude of the Ca^{2+} transients evoked by both single (77.2 ± 9.5%, $P < 0.05$) and triple (72.9 ± 9.1%, $P < 0.01$) stimuli (**Fig. 3b,d**). In contrast, selective blockade of R-type channels with SNX-482 produced a significant increase in average ($n = 20$) uEPSP magnitude ($P < 0.001$; **Fig. 3b,c**). These results suggest that, similar to the hippocampus, blocking R-type channels disengages a negative feedback loop involving SK channels, thereby boosting synaptic potentials and NMDAR-mediated Ca^{2+} influx[23]. The lack of uEPSP boosting and the reduction in burst-evoked uEPSPs by mibefradil suggests that the broad actions of this nonselective agent may influence the generation of synaptic potentials. In summary, our results indicate that the largest fraction of spine Ca^{2+} influx evoked by activation of a single postsynaptic terminal in striatopallidal MSNs arises from NMDAR opening, with additional contributions from R- and either T- or dihydropyridine-resistant L-type VGCCs, and suggest that these sources are potential targets for dopaminergic control of synaptic Ca^{2+} influx.

D2Rs inhibit NMDAR- and R-type VGCC-mediated Ca^{2+} influx

To examine the potential modulation of NMDAR-mediated synaptic responses, we voltage-clamped MSNs at −70 mV using a cesium-based internal solution and bathed them in artificial cerebrospinal fluid (ACSF) containing nominally zero extracellular Mg^{2+}, tetrodotoxin, a full cocktail of VGCC antagonists (Online Methods) and the AMPA-type glutamate receptor (AMPAR) antagonist
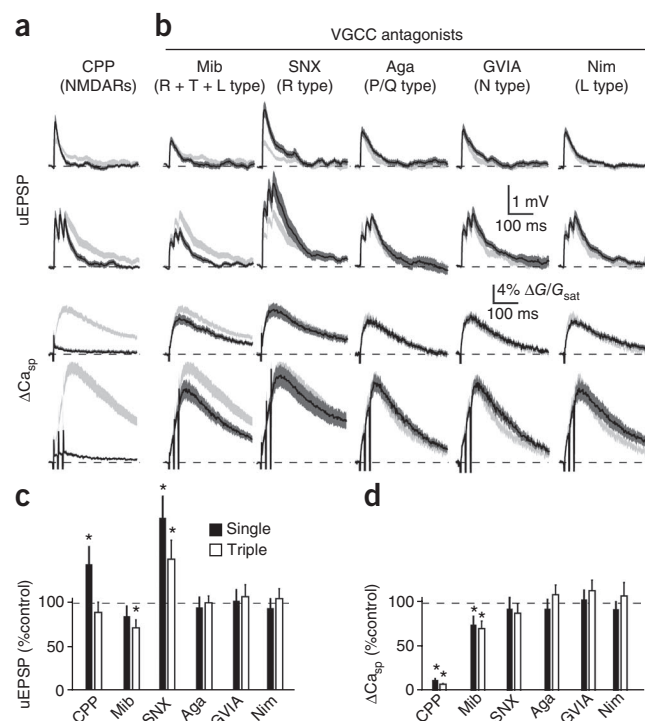
6-nitro-2,3-dioxo-1,4-dihydrobenzo[f]quinoxaline-7-sulfonamide (NBQX). Under these conditions, glutamate uncaging evoked an average ($n = 30$) excitatory postsynaptic current (uEPSC, 13.0 ± 1.4 pA) and associated Ca^{2+} transient in the spine head ($\Delta G_{sp}/G_{sat} = 26.5 ± 3.0\%$; **Fig. 4a**). Activation of D2Rs produced no change in the average ($n = 27$) NMDAR-mediated uEPSC (11.1 ± 1.3 pA, $P = 0.31$), but significantly decreased the Ca^{2+} transient ($\Delta G_{sp}/G_{sat} = 17.0 ± 2.1\%$, $P < 0.05$; **Fig. 4a**). We performed a similar analysis for nonNMDAR-mediated responses using ACSF with control Mg^{2+} concentration and in the presence of the NMDAR antagonist CPP. The average ($n = 19$) nonNMDAR-mediated uEPSC (26.0 ± 3.6 pA) and associated Ca^{2+} transient ($\Delta G_{sp}/G_{sat} = 0.7 ± 0.1\%$) were not altered in the presence of quinpirole ($n = 16$; 30.2 ± 2.9 pA, $P = 0.39$; $\Delta G_{sp}/G_{sat} = 0.8 ± 0.1\%$, $P = 0.62$; **Fig. 4b**), indicating that D2Rs selectively reduce Ca^{2+} accumulation resulting from activation of NMDARs.

We determined the actions of D2Rs on VGCCs by examining the modulation of Ca^{2+} transients evoked by back-propagating action potentials (bAPs; **Fig. 5a**). On average ($n = 30$), a single bAP evoked by brief somatic current injection resulted in Ca^{2+} influx in the spine head ($\Delta G_{sp}/G_{sat} = 8.8 ± 0.01\%$) and neighboring dendrite ($\Delta G_{den}/G_{sat} = 6.7 ± 0.4\%$; **Fig. 5b**). During a brief burst of three bAPs, Ca^{2+} was further increased in both compartments
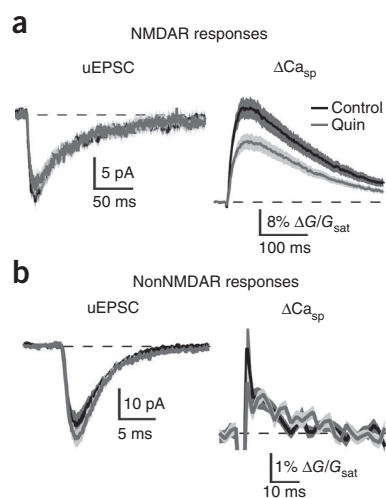
Figure 4 Activation of D2Rs modulates NMDAR-mediated, but not nonNMDAR-mediated, synaptic responses. (**a**) Uncaging-evoked NMDAR-mediated uEPSCs (left) and ΔCa_{sp} (right) recorded in voltage clamp in the presence of nominally zero extracellular Mg, the AMPAR antagonist NBQX and a cocktail of VGCC blockers. Mean (solid lines) and mean ± s.e.m. (shaded regions) are shown for responses in control conditions (black, $n = 30$) and in the presence of quinpirole (gray, $n = 27$). (**b**) Uncaging-evoked nonNMDAR-mediated uEPSCs (left) and ΔCa_{sp} (right) recorded in the presence of normal extracellular Mg, the NMDAR antagonist CPP and a cocktail of VGCC blockers. Mean (solid lines) and mean ± s.e.m. (shaded regions) are shown for responses in control conditions (black, $n = 19$) and in the presence of quinpirole (gray, $n = 16$).

Figure 5 Activation of D2Rs modulates R-type VGCCs. (**a**) Top, two-photon laser-scanning microscopy image of a striatopallidal MSN dendrite filled with Alexa Fluor 594 and Fluo 5F. Bottom, red and green fluorescence in the spine head (sp) and neighboring dendrite (den) measured in line scan over the region indicated by the dashed line in the upper image. The Ca^{2+}-dependent increase in green fluorescence was evoked by a single action potential generated by somatic current injection. The somatic action potential and associated ΔCa_{sp} are shown below (white traces). Inset scale bars represent 10 mV, 8% $\Delta G/G_{sat}$, 50 ms. (**b**) bAP-evoked ΔCa_{sp} (left) and ΔCa_{den} (right) produced by either single or triple (50 Hz) bAPs are shown for control conditions (black, $n = 30$) or in the presence of quinpirole (gray, $n = 34$). Mean (solid lines) and mean ± s.e.m. (shaded regions) are shown. (**c**) Population data for ΔCa_{sp}, expressed as a percentage of the control value, for single and triple bAP-evoked responses measured in the presence of drugs as indicated: mibefradil (Mib, $n = 24$), SNX-482 (SNX, $n = 23$), ω-agatoxin IVA (Aga, $n = 23$), ω-conotoxin GVIA (GVIA, $n = 22$), nimodipine (Nim, $n = 20$), quinpirole alone ($n = 34$), quinpirole + mibefradil ($n = 25$) and quinpirole + SNX-482 ($n = 23$). (**d**) Data are presented as in **c** for ΔCa_{den}.

($\Delta G_{sp}/G_{sat} = 22.0 \pm 1.6\%$, $\Delta G_{den}/G_{sat} = 17.4 \pm 1.2\%$; **Fig. 5b** and **Supplementary Fig. 2**). Activation of D2Rs reduced the average ($n = 34$) bAP-evoked Ca^{2+} transient for both single ($\Delta G_{sp}/G_{sat} = 5.4 \pm 0.5\%$, $P < 0.0001$; $\Delta G_{den}/G_{sat} = 4.2 \pm 0.4\%$, $P < 0.0001$) and triple ($\Delta G_{sp}/G_{sat} = 15.0 \pm 1.2\%$, $P < 0.001$; $\Delta G_{den}/G_{sat} = 11.9 \pm 0.9\%$, $P < 0.001$; **Fig. 5b–d**) stimuli, suggesting that VGCCs are targets of D2R modulation. Quinpirole did not alter the temporal summation (**Supplementary Fig. 2**) or exponential decay time constants of the bAP-evoked spine Ca^{2+} transients (75.6 ± 6.3 ms versus 82.6 ± 9.4 ms for control and quinpirole, respectively, $P = 0.55$), suggesting a lack of effect on Ca^{2+} clearance.

In the presence of mibefradil, the average ($n = 24$) single bAP-evoked Ca^{2+} signal was reduced to 33.4 ± 2.8% ($P < 0.0001$) and 42.6 ± 3.9% ($P < 0.0001$) of control values for spines and dendrites, respectively, indicating a large contribution of R-, T- and/or L-type channels (**Fig. 5c,d**). The selective R-type blocker SNX-482 also reduced single bAP-evoked Ca^{2+} influx to 70.0 ± 5.6% ($n = 23$, $P < 0.0001$) and 77.8 ± 7.3% ($P < 0.01$) of control values for spines and dendrites, respectively (**Fig. 5c,d**). In contrast, there was no change in Ca^{2+} influx in the presence of ω-agatoxin IVA ($n = 23$), ω-conotoxin-GVIA ($n = 22$) or 3 µM nimodipine ($n = 20$) (**Fig. 5c,d**). Similar results were seen following bursts of three bAPs (**Fig. 5c,d**), and none of the VGCC blockers altered the temporal summation of bAP-evoked Ca^{2+} signals (**Supplementary Fig. 2**). These results suggest that R-type as well as T- and/or dihydropyridine-resistant L-type channels contribute to bAP-evoked Ca^{2+} influx.

We next examined the ability of mibefradil and SNX-482 to mimic and occlude the actions of quinpirole (**Fig. 5c,d**). A one-way ANOVA revealed significant differences between the effects of mibefradil, SNX-482, quinpirole alone and each of the VGCC blockers in the presence of quinpirole ($F = 13.26$, $P < 0.0001$ and $F = 11.30$, $P < 0.0001$ for spines and dendrites, respectively) on single bAP-evoked Ca^{2+} transients. Tukey's multiple *post hoc* comparisons revealed that SNX-482 mimicked and occluded the actions of quinpirole, while mibefradil produced a significantly larger reduction in Ca^{2+} influx than either SNX-482 or quinpirole alone (comparisons significant for $P < 0.05$). Similar results were obtained for the triple bAP stimuli, arguing that D2Rs modulate R-type VGCCs, with minimal effect on T- or L-type channels.

Previous studies have linked dopaminergic regulation of $Ca_V1.3$ L-type channels with MSN spine stability[31]. To examine whether these channels were present, but either inactive or insensitive to dihydropyridine block[30], during brief synaptic or bAP stimuli, we measured
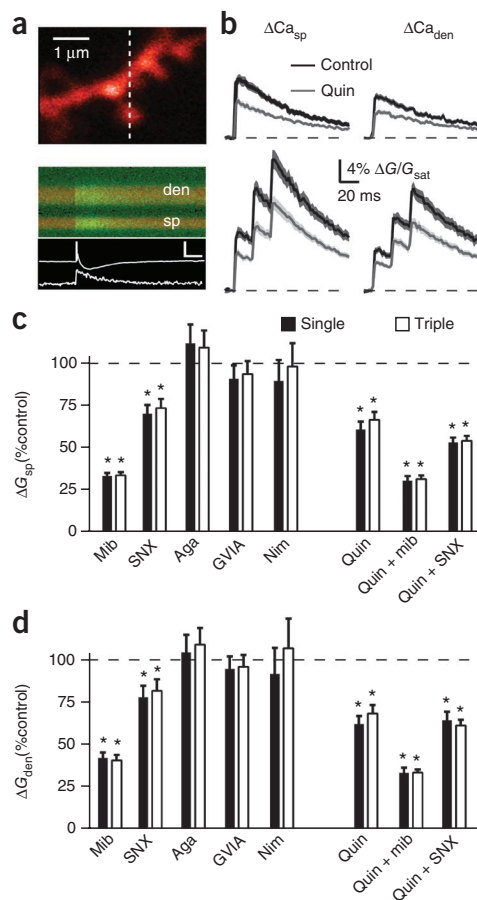
spine Ca^{2+} influx during 300-ms voltage steps from −70 to 0 mV (**Fig. 6a**). In the presence of blockers for R-, N- and P/Q-type VGCCs, we observed a large Ca^{2+} transient that rapidly reached steady state and decayed following return of the holding potential to baseline. Nimodipine (3 µM) reduced the step-evoked transients from 60.2 ± 2.4% ($n = 22$) to 43.7 ± 2.2% ($n = 21$) (**Fig. 6b**). Activation of D2Rs decreased the amplitude to 36.7 ± 1.4% ($n = 20$), whereas coapplication of quinpirole and nimodipine produced an additional reduction to 21.4 ± 2.6% ($n = 20$; **Fig. 6b**). A one-way ANOVA comparing control, quinpirole, nimodipine and both quinpirole and nimodipine revealed significant differences between these groups ($F = 54.6$, $P < 0.0001$). *Post hoc* analysis revealed that quinpirole and nimodipine both significantly reduced Ca^{2+} influx relative to control and that the two together produced significantly greater reduction than either alone (comparisons significant for $P < 0.05$). However, calculation of the nimodipine-sensitive component (the arithmetic difference between pre- and post-nimodipine values) indicated that the contribution of L-type VGCCs was unaffected by quinpirole (16.5 ± 2.3% versus 15.3 ± 2.1% $\Delta G/G_{sat}$, in control and quinpirole, respectively, $P > 0.05$). In summary, our data indicate that R-, L- and T-type VGCCs are present in MSN spines, although R-types are the primary channel regulated by D2Rs.

D2Rs act via PKA-dependent and PKA-independent pathways

Studies in hippocampal neurons have indicated that a PKA-dependent mechanism augments Ca^{2+} influx through NMDARs without altering total current flow[32]. We therefore examined whether D2R-mediated inhibition of PKA is responsible for the reduction in NMDAR-mediated Ca^{2+} influx. We isolated NMDAR-mediated responses as

Figure 6 Voltage-steps reveal L-type Ca^{2+} channels in MSN spines.
(**a**) Left, two-photon laser-scanning microscopy image of a striatopallidal MSN dendrite filled with Alexa Fluor 594 and Fluo 5F. Right, red and green fluorescence in the spine head (sp) and neighboring dendrite (den) measured in line scan over the region indicated by the dashed line at left. The increase in Ca^{2+}-dependent green fluorescence was evoked by a 300-ms voltage step from –70 mV to 0 mV at the time indicated by the white line. (**b**) Left, mean ± s.e.m. (shaded traces) are shown for responses evoked under control conditions ($n = 22$, black) and in the presence of nimodipine ($n = 21$, gray). Right, mean ± s.e.m. for responses evoked in the presence of quinpirole ($n = 20$, black) or quinpirole + nimodipine ($n = 20$, gray).

described above and tested the ability of PKI(14-22), a membrane-permeable specific antagonist of PKA, to mimic and occlude the actions of quinpirole. In the presence of PKI(14-22), the average ($n = 21$) NMDAR-mediated uEPSC was 13.0 ± 1.6 pA and the associated spine Ca^{2+} transient was 15.8 ± 2.0% and 6.9 ± 1.2% (**Fig. 7a,b**). Similar results were found using the alternate PKA antagonist H89 ($n = 19$; **Fig. 7b**). Following coapplication of PKI(14-22) and quinpirole ($n = 20$), the uEPSC was 14.9 ± 2.3 pA and the Ca^{2+} signal was 15.1 ± 1.7% (**Fig. 7a,b**). A one-way ANOVA comparing control, PKI(14-22), quinpirole and both PKI(14-22) and quinpirole revealed significant differences for Ca^{2+} transients between these groups ($F = 6.14$, $P < 0.01$). *Post hoc* comparisons showed significant differences between control and PKI(14-22), as well as between control and both PKI(14-22) and quinpirole, whereas there was no difference between quinpirole alone and in combination with PKI(14-22) (comparisons significant for $P < 0.05$). Thus, antagonism of PKA is sufficient to mimic and occlude the actions of D2Rs on NMDAR-mediated Ca^{2+} transients.

Striatopallidal MSNs also express A2ARs, which are positively coupled to PKA via $G\alpha_s$[7] and oppose the actions of D2Rs on long-term synaptic plasticity in the striatum[19]. We examined whether these two modulatory pathways also interact in the control of NMDAR-mediated Ca^{2+} influx. Application of the specific A2AR agonist CGS-21680 ($n = 16$) resulted in a uEPSC magnitude of 27.8 ± 4.5 pA and a spine Ca^{2+} transient of 28.5 ± 3.2% (**Fig. 7a,b**). Coapplication of CGS-21680 and quinpirole ($n = 15$) resulted in a uEPSC magnitude of 22.7 ± 3.0 pA and spine Ca^{2+} transient of 29.5 ± 3.0% (**Fig. 7a,b**). A one-way ANOVA comparing control, quinpirole, CGS-21680 and both CGS-21680 and quinpirole revealed significant differences between these groups ($F = 3.9$, $P < 0.05$). *Post hoc* analyses indicated that the uEPSC
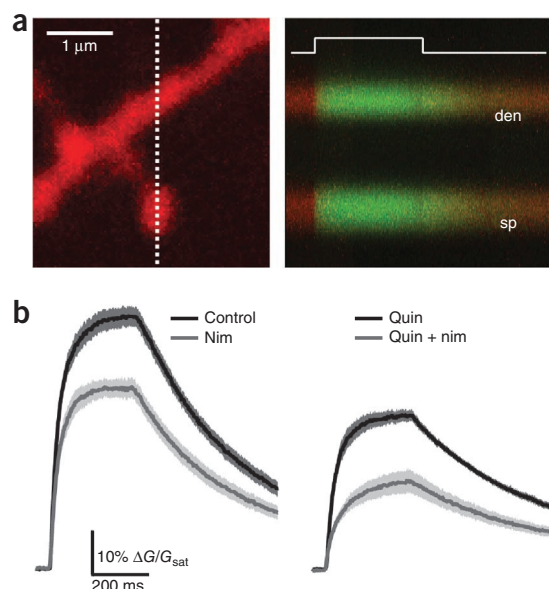
magnitudes for A2AR and combined A2AR and D2R activation were significantly increased, whereas spine Ca^{2+} transients did not differ from control values (significant for $P < 0.05$).

We next examined whether basal activation of A2ARs influences Ca^{2+} influx through NMDARs. Application of the specific A2AR antagonist SCH-58261 ($n = 19$) resulted in a uEPSC magnitude of 8.8 ± 1.8 pA and a spine Ca^{2+} transient of 8.5 ± 0.7% (**Fig. 7b**). Coapplication of SCH-58261 and quinpirole ($n = 18$) resulted in a uEPSC magnitude of 7.6 ± 1.7 pA and a spine Ca^{2+} transient of 12.7 ± 2.3% (**Fig. 7b**). A one-way ANOVA with *post hoc* tests comparing control, quinpirole, SCH-58261 and both SCH-58261 and quinpirole revealed no significant change in uEPSC magnitude ($F = 2.521$, $P = 0.063$). However, A2AR antagonism alone or in combination with quinpirole significantly reduced synaptic Ca^{2+} influx, whereas there was no difference between these two groups (significant for $P < 0.05$). In summary, basal levels of A2AR activation enhance Ca^{2+} influx through NMDARs and reduction of this activity is sufficient to mimic and occlude the effects of D2R activation. Furthermore, exogenous activation of A2ARs can counteract the D2R-mediated, PKA-dependent reduction in synaptic Ca^{2+} influx, suggesting that modulatory control of PKA exerts a bidirectional influence on NMDAR Ca^{2+} signaling.

In the hippocampus, NMDARs containing the NR2B-type subunit contribute to particularly large Ca^{2+} influx[33], and removal of these subunits might explain the reduction in synaptic Ca^{2+} influx. However, application of the selective NR2B-containing NMDAR
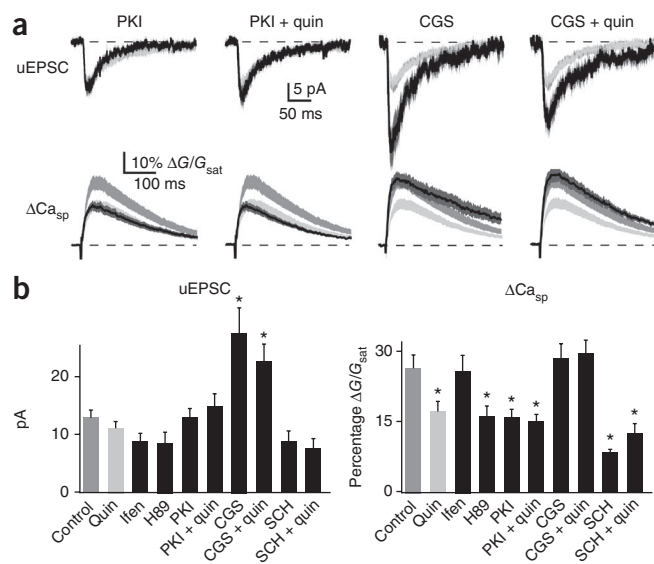

Figure 7 Push-pull modulation of NMDARs by D2Rs and A2ARs is dependent on PKA activity. (**a**) Uncaging-evoked NMDAR-mediated uEPSCs (upper traces) and ΔCa_{sp} (lower traces), recorded as in **Figure 4a**. Mean (black solid lines) and mean ± s.e.m. (dark gray shaded regions) are shown for responses evoked in the presence of the PKA antagonist PKI(14-22) alone (first column, $n = 21$), PKI(14-22) + quinpirole (second column, $n = 20$), the A2AR agonist CGS-21680 alone (third column, $n = 16$) or CGS-21680 + quinpirole (fourth column, $n = 15$). Medium gray and light gray shaded regions indicate the mean ± s.e.m. responses under control and quinpirole conditions, respectively, reproduced from **Figure 4a** for comparison. (**b**) Population data for peak uEPSC (left) and ΔCa_{sp} (right) are shown for the conditions illustrated in **a**. Also shown are the population data for the PKA antagonist H89, the NR2B subunit–containing NMDAR antagonist ifenprodil, the A2AR antagonist SCH-58261, and SCH-58261 + quinpirole. *$P < 0.05$.

Figure 8 Modulation of VGCCs by D2Rs is independent of A2AR and PKA activity. (**a**) bAP-evoked ΔCa_{sp} (upper traces) and ΔCa_{den} (lower traces) recorded as in **Figure 5b**. Mean (black solid lines) and mean ± s.e.m. (dark gray shaded regions) are shown for responses evoked in the presence of PKI(14-22) alone (left, $n = 20$), PKI(14-22) + quinpirole (middle, $n = 17$) or CGS-21680 + quinpirole (right, $n = 11$). Medium gray and light gray shaded regions indicate the mean ± s.e.m. responses under control and quinpirole conditions, respectively, reproduced from **Figure 5b** for comparison. (**b**) Population data for ΔCa_{sp} (left) and ΔCa_{den} (right) are shown for the conditions illustrated in **a**. *$P < 0.05$.
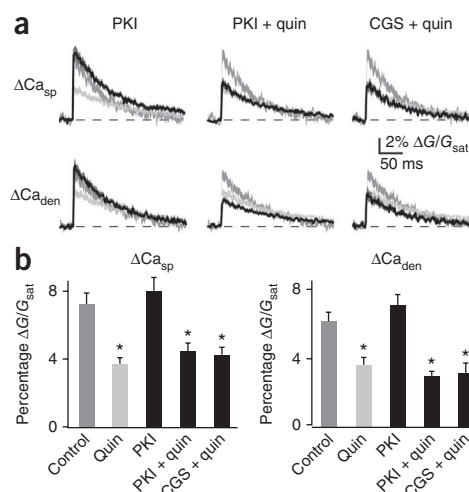
antagonist ifenprodil ($n = 18$) revealed no significant change in uEPSC or Ca^{2+} transient magnitude ($P < 0.05$; **Fig. 7b**), suggesting that this subgroup of receptors does not contribute substantially to Ca^{2+} influx under control conditions.

Finally, we examined whether similar PKA-dependent mechanisms underlie the D2R-mediated reduction in bAP-evoked Ca^{2+} signals. A one-way ANOVA revealed significant differences between spine Ca^{2+} transients in control, quinpirole, PKI(14-22) ($n = 20$), PKI(14-22) and quinpirole ($n = 17$), and CGS-21680 and quinpirole ($n = 11$) ($F = 10.3$, $P < 0.0001$; **Fig. 8a,b**). *Post hoc* tests indicated that, in the presence of PKI(14-22), Ca^{2+} influx did not significantly differ from control conditions. Furthermore, coapplication of quinpirole and either PKI(14-22) or CGS-21680 produced a reduction in signal that did not differ from that seen with quinpirole alone (all comparisons significant for $P < 0.05$). Similar results were obtained for dendrite Ca^{2+} signals (**Fig. 8a,b**). These findings indicate that the actions of D2Rs on bAP-evoked VGCC-mediated Ca^{2+} transients occur independently of PKA and A2AR activation and suggest that D2Rs couple to two independent pathways that converge on a similar endpoint of reduced Ca^{2+} signaling in dendritic spines.

DISCUSSION

Perturbation of D2R-dependent dopaminergic modulation in the striatum is linked to a variety of neuropsychiatric disorders, including Parkinson's disease, obsessive-compulsive disorder and, most notably, schizophrenia[2,4]. Schizophrenic individuals show evidence of increased density and occupancy of striatal D2Rs[34], and most effective antipsychotic agents antagonize D2Rs[5,35]. Furthermore, overexpression of striatal D2Rs in mice produces behavioral impairments that are thought to model those seen in schizophrenic individuals[36]. We found that activation of D2Rs reduced glutamate release from cortical afferents and attenuated Ca^{2+} influx through NMDARs. The regulation of NMDAR Ca^{2+} signaling occurs via a reduction in PKA activity and can be prevented by coactivation of A2ARs. D2Rs also act via a PKA-independent pathway to reduce Ca^{2+} signaling through SNX-482–sensitive R-type ($Ca_V2.3$) VGCCs. Thus, our results indicate that D2R activation triggers divergent signaling cascades that inhibit multiple synaptic Ca^{2+} sources. Furthermore, we provide evidence of a functional synaptic role for D2R- and A2AR-mediated regulation of PKA, implicating this kinase as a target for convergent neuromodulatory control over NMDAR-mediated Ca^{2+} signaling and a likely substrate for control of synaptic plasticity in the striatum.

Regulation of corticostriatal glutamate release

By using mice in which corticostriatal afferents expressed light-activatable ChR2, we were able to selectively characterize the D2R-mediated modulation of cortical inputs to striatopallidal MSNs. Consistent with the results of previous studies, activation of D2Rs reduced the magnitude of evoked postsynaptic potentials and currents[11]. Coupled with the observation that D2Rs failed to alter

uncaging-evoked synaptic potentials or currents, our data strongly support the hypothesis that D2Rs regulate corticostriatal transmission by reducing glutamate release from afferent terminals[10,11]. However, we cannot conclude whether pre- or postsynaptic D2Rs, possibly coupled to retrograde endocannabinoid signaling, mediate this phenomenon[10,11,37].

In contrast, we found no evidence for direct modulation of postsynaptic nonNMDA-type glutamate receptors. Notably, experiments using electrical stimuli revealed no modulation of glutamatergic responses, suggesting that such stimulation may evoke dopamine release from the terminals of nigrostriatal afferents, thereby occluding the effects of exogenously applied agonists[11].

Sources of synaptic Ca^{2+} influx in striatopallidal MSNs

Our data reveal that, following either single or burst stimulation of an individual synapse, NMDARs contribute the bulk of Ca^{2+} influx, although both Ca^{2+}-permeable AMPARs and VGCCs make additional contributions. However, in contrast with hippocampal pyramidal cells[33], we found little contribution of NR2B-containing NMDARs. Similar to hippocampal and cortical pyramidal neurons (reviewed in ref. 38), the major VGCC contributors to synaptic or bAP-evoked spine Ca^{2+} influx are SNX-482– and mibefradil-sensitive channels. Although SNX-482 specifically indicates the presence of R-type ($Ca_V2.3$) VGCCs, the nonselective mibefradil suggests contributions from T-type (Ca_V3) and/or L-type ($Ca_V1.2$ and 1.3) channels. Using large voltage steps to directly depolarize the spine, we found a nimodipine-sensitive Ca^{2+} transient, confirming that L-type VGCCs are present in MSN spines[31]. However, these channels either contribute little to synaptic Ca^{2+} influx or are not effectively blocked by nimodipine during brief depolarizations[30].

An unexpected finding is that blocking either NMDARs or R-type VGCCs increased uEPSP magnitude, a result mimicked by blocking SK-type Ca^{2+}-activated potassium channels. In the hippocampus and amygdala, Ca^{2+} influx through these two sources and subsequent opening of SK channels produces local hyperpolarization and inhibits synaptic responses[23,27]. Our data suggest that SK channels may have a similar feedback role in MSNs. Notably, quinpirole reduced Ca^{2+} influx through both NMDARs and R-type VGCCs, but did not augment the uEPSP, suggesting that D2Rs may directly regulate SK activation.

Regulation of spine Ca^{2+} signaling by D2Rs

We found that activation of D2Rs reduced synaptically evoked spine Ca^{2+} transients mediated by NMDARs. This effect could result

from a D2R-mediated reduction in the number of NR2B-containing receptors, which exhibit a higher fractional Ca^{2+} permeability[33]. However, the failure of ifenprodil to alter synaptic Ca^{2+} transients suggests that these receptors do not contribute substantially under control conditions. Alternatively, D2Rs may regulate NMDAR Ca^{2+} permeability, consistent with previous studies indicating that fractional permeability for divalent ions can be modified by phosphorylation or structural changes[32,39]. Such mechanisms may also be developmentally regulated, as studies in other brain regions indicate that relative NR2B expression levels and PKA-dependent modulation of NMDAR Ca^{2+} permeability are greater in young animals[32,40]. As our experiments were performed in juvenile mice, it will be important to determine whether D2R actions on striatal NMDARs are similarly developmentally regulated.

Modulation of NMDAR Ca^{2+} transients was mimicked and occluded by pharmacologically inhibiting PKA activity, consistent with the biochemical coupling of D2Rs to $G\alpha_i$ and downstream inhibition of cAMP generation and PKA activity[6]. Moreover, blocking the activity of A2ARs, which are positively coupled to cAMP production and PKA activity via $G\alpha_s$[7], similarly reduced NMDAR Ca^{2+} influx and occluded the actions of quinpirole. Furthermore, the actions of D2Rs were prevented by coapplication of an A2AR agonist. These results suggest that basal A2AR tone facilitates NMDAR-mediated Ca^{2+} entry, but D2Rs and A2ARs act competitively to control synaptic Ca^{2+} influx. Activation of A2ARs also boosted the uEPSC amplitude, possibly reflecting enhancement of current through extrasynaptic receptors. Notably, although biochemical experiments have shown that PKA may increase phosphorylation of both AMPARs and NMDARs either directly or indirectly via DARPP-32–dependent inhibition of protein phosphatase 1 (refs. 41,42), our results provide, to the best of our knowledge, the first description of a functional consequence for D2R- or A2AR-mediated control of PKA on synaptic transmission. D2R signaling via release of $G_{\beta\gamma}$ subunits is known to produce a membrane-delimited PLC- and calcineurin-dependent inhibition of whole-cell Ca^{2+} currents through VGCCs[12,13]. This alternative pathway may underlie the previously reported D2R-mediated reduction in bAP-evoked Ca^{2+} influx[43] and is consistent with our finding that inhibition of R-type VGCCs was independent of PKA activity. Although reduction in dendritic excitability might also decrease bAP-evoked Ca^{2+} influx through VGCCs by limiting local depolarization[43], our analysis of relatively proximal spines (<60 µM from the soma) suggests this mechanism is unlikely to explain our findings. Nevertheless, it is possible that dopaminergic modulation may be different in more distal dendritic regions.

Implications for striatal plasticity

Plasticity of glutamatergic synapses in the striatum is thought to represent an important substrate for both normal and pathological motor learning and is strongly regulated by dopaminergic activity[2,44]. In striatopallidal neurons, activation of D2Rs during pairing of pre- and postsynaptic activity is sufficient to convert NMDAR-dependent LTP into LTD, and this switch is prevented by coactivation of A2ARs[19]. Our finding that D2R and A2AR activities bidirectionally control NMDAR-mediated Ca^{2+} influx provides a potential mechanism for these observations. Notably, striatal LTD, which is dependent on the activation of postsynaptic metabotropic glutamate receptors, Ca^{2+} influx through L-type VGCCs and retrograde endocannabinoid signaling, is disrupted by antagonism of D2Rs[16,20,21]. In addition, both genetic and pharmacological deletion of D2R signaling converts LTD into LTP[16,19]. However, the mechanisms underlying D2R control of

LTD are unclear. One hypothesis suggests that D2Rs enhance the release of endocannabinoids from spines via a $G_{\beta\gamma}$-dependent activation of PLC, leading to retrograde inhibition of glutamate release[11,20,45]. This possibility is supported by our observation that D2R-mediated inhibition of VGCCs occurs via a PKA-independent pathway. Thus, we propose a model of striatal long-term plasticity in which NMDAR-dependent LTP and endocannabinoid-dependent LTD compete to determine net synaptic strength. In this model, D2Rs tip the balance in favor of depression by simultaneously reducing NMDAR-mediated Ca^{2+} influx via a PKA-dependent process, reducing VGCC-mediated Ca^{2+} influx and likely enhancing endocannabinoid production via PKA-independent signaling. In summary, our findings highlight the existence of local neuromodulatory actions on synaptic transmission and provide new insight into the role of dopaminergic modulation in the striatum.

METHODS

Methods and any associated references are available in the online version of the paper at http://www.nature.com/natureneuroscience/.

Note: Supplementary information is available on the Nature Neuroscience website.

AUTHOR CONTRIBUTIONS
M.J.H. conducted the experiments and data analysis. M.J.H. and B.L.S. designed the experiments and wrote the manuscript.

1. Graybiel, A.M. The basal ganglia. *Curr. Biol.* **10**, R509–R511 (2000).
2. Kreitzer, A.C. & Malenka, R.C. Striatal plasticity and basal ganglia circuit function. *Neuron* **60**, 543–554 (2008).
3. Surmeier, D.J., Ding, J., Day, M., Wang, Z. & Shen, W. D1 and D2 dopamine-receptor modulation of striatal glutamatergic signaling in striatal medium spiny neurons. *Trends Neurosci.* **30**, 228–235 (2007).
4. Bonci, A. & Hopf, F.W. The dopamine D2 receptor: new surprises from an old friend. *Neuron* **47**, 335–338 (2005).
5. Meltzer, H.Y. What's atypical about atypical antipsychotic drugs? *Curr. Opin. Pharmacol.* **4**, 53–57 (2004).
6. Missale, C., Nash, S.R., Robinson, S.W., Jaber, M. & Caron, M.G. Dopamine receptors: from structure to function. *Physiol. Rev.* **78**, 189–225 (1998).
7. Schiffmann, S.N., Fisone, G., Moresco, R., Cunha, R.A. & Ferre, S. Adenosine A2A receptors and basal ganglia physiology. *Prog. Neurobiol.* **83**, 277–292 (2007).
8. Hersch, S.M. *et al.* Electron microscopic analysis of D1 and D2 dopamine receptor proteins in the dorsal striatum and their synaptic relationships with motor corticostriatal afferents. *J. Neurosci.* **15**, 5222–5237 (1995).
9. Cepeda, C., Buchwald, N.A. & Levine, M.S. Neuromodulatory actions of dopamine in the neostriatum are dependent upon the excitatory amino acid receptor subtypes activated. *Proc. Natl. Acad. Sci. USA* **90**, 9576–9580 (1993).
10. Bamford, N.S. *et al.* Dopamine modulates release from corticostriatal terminals. *J. Neurosci.* **24**, 9541–9552 (2004).
11. Yin, H.H. & Lovinger, D.M. Frequency-specific and D2 receptor–mediated inhibition of glutamate release by retrograde endocannabinoid signaling. *Proc. Natl. Acad. Sci. USA* **103**, 8251–8256 (2006).
12. Hernandez-Lopez, S. *et al.* D2 dopamine receptors in striatal medium spiny neurons reduce L-type Ca2+ currents and excitability via a novel PLC[beta]1–IP3-calcineurin-signaling cascade. *J. Neurosci.* **20**, 8987–8995 (2000).

13. Olson, P.A. *et al.* G-protein-coupled receptor modulation of striatal CaV1.3 L-type Ca2+ channels is dependent on a Shank-binding domain. *J. Neurosci.* **25**, 1050–1062 (2005).
14. Salgado, H. *et al.* A reconfiguration of CaV2 Ca2+ channel current and its dopaminergic D2 modulation in developing neostriatal neurons. *J. Neurophysiol.* **94**, 3771–3787 (2005).
15. Wang, Z. *et al.* Dopaminergic control of corticostriatal long-term synaptic depression in medium spiny neurons is mediated by cholinergic interneurons. *Neuron* **50**, 443–452 (2006).
16. Calabresi, P. *et al.* Abnormal synaptic plasticity in the striatum of mice lacking dopamine D2 receptors. *J. Neurosci.* **17**, 4536–4544 (1997).
17. Pawlak, V. & Kerr, J.N. Dopamine receptor activation is required for corticostriatal spike-timing–dependent plasticity. *J. Neurosci.* **28**, 2435–2446 (2008).
18. Kreitzer, A.C. & Malenka, R.C. Endocannabinoid-mediated rescue of striatal LTD and motor deficits in Parkinson's disease models. *Nature* **445**, 643–647 (2007).
19. Shen, W., Flajolet, M., Greengard, P. & Surmeier, D.J. Dichotomous dopaminergic control of striatal synaptic plasticity. *Science* **321**, 848–851 (2008).
20. Kreitzer, A.C. & Malenka, R.C. Dopamine modulation of state-dependent endocannabinoid release and long-term depression in the striatum. *J. Neurosci.* **25**, 10537–10545 (2005).
21. Ronesi, J. & Lovinger, D.M. Induction of striatal long-term synaptic depression by moderate frequency activation of cortical afferents in rat. *J. Physiol. (Lond.)* **562**, 245–256 (2005).
22. Heintz, N. BAC to the future: the use of bac transgenic mice for neuroscience research. *Nat. Rev. Neurosci.* **2**, 861–870 (2001).
23. Bloodgood, B.L. & Sabatini, B.L. Nonlinear regulation of unitary synaptic signals by CaV(2.3) voltage-sensitive calcium channels located in dendritic spines. *Neuron* **53**, 249–260 (2007).
24. Busetto, G., Higley, M.J. & Sabatini, B.L. Developmental presence and disappearance of postsynaptically silent synapses on dendritic spines of rat layer 2/3 pyramidal neurons. *J. Physiol. (Lond.)* **586**, 1519–1527 (2008).
25. Carter, A.G., Soler-Llavina, G.J. & Sabatini, B.L. Timing and location of synaptic inputs determine modes of subthreshold integration in striatal medium spiny neurons. *J. Neurosci.* **27**, 8967–8977 (2007).
26. Higley, M.J., Soler-Llavina, G.J. & Sabatini, B.L. Cholinergic modulation of multivesicular release regulates striatal synaptic potency and integration. *Nat. Neurosci.* **12**, 1121–1128 (2009).
27. Faber, E.S., Delaney, A.J. & Sah, P. SK channels regulate excitatory synaptic transmission and plasticity in the lateral amygdala. *Nat. Neurosci.* **8**, 635–641 (2005).
28. Carter, A.G. & Sabatini, B.L. State-dependent calcium signaling in dendritic spines of striatal medium spiny neurons. *Neuron* **44**, 483–493 (2004).
29. Furukawa, T. *et al.* Five different profiles of dihydropyridines in blocking T-type Ca^{2+} channel subtypes (Ca(v)3.1 (alpha1G), Ca(v)3.2 (alpha1H), and Ca(v)3.3 (alpha1I)) expressed in *Xenopus* oocytes. *Eur. J. Pharmacol.* **613**, 100–107 (2009).
30. Lipscombe, D., Helton, T.D. & Xu, W. L-type calcium channels: the low down. *J. Neurophysiol.* **92**, 2633–2641 (2004).
31. Day, M. *et al.* Selective elimination of glutamatergic synapses on striatopallidal neurons in Parkinson disease models. *Nat. Neurosci.* **9**, 251–259 (2006).
32. Skeberdis, V.A. *et al.* Protein kinase A regulates calcium permeability of NMDA receptors. *Nat. Neurosci.* **9**, 501–510 (2006).
33. Sobczyk, A., Scheuss, V. & Svoboda, K. NMDA receptor subunit-dependent [Ca^{2+}] signaling in individual hippocampal dendritic spines. *J. Neurosci.* **25**, 6037–6046 (2005).
34. Wong, D.F. *et al.* Positron emission tomography reveals elevated D2 dopamine receptors in drug-naive schizophrenics. *Science* **234**, 1558–1563 (1986).
35. Seeman, P. & Lee, T. Antipsychotic drugs: direct correlation between clinical potency and presynaptic action on dopamine neurons. *Science* **188**, 1217–1219 (1975).
36. Drew, M.R. *et al.* Transient overexpression of striatal D2 receptors impairs operant motivation and interval timing. *J. Neurosci.* **27**, 7731–7739 (2007).
37. Wang, H. & Pickel, V.M. Dopamine D2 receptors are present in prefrontal cortical afferents and their targets in patches of the rat caudate-putamen nucleus. *J. Comp. Neurol.* **442**, 392–404 (2002).
38. Higley, M.J. & Sabatini, B.L. Calcium signaling in dendrites and spines: practical and functional considerations. *Neuron* **59**, 902–913 (2008).
39. Burnashev, N. *et al.* Control by asparagine residues of calcium permeability and magnesium blockade in the NMDA receptor. *Science* **257**, 1415–1419 (1992).
40. Hoffmann, H., Gremme, T., Hatt, H. & Gottmann, K. Synaptic activity-dependent developmental regulation of NMDA receptor subunit expression in cultured neocortical neurons. *J. Neurochem.* **75**, 1590–1599 (2000).
41. Håkansson, K. *et al.* Regulation of phosphorylation of the GluR1 AMPA receptor by dopamine D2 receptors. *J. Neurochem.* **96**, 482–488 (2006).
42. Westphal, R.S. *et al.* Regulation of NMDA receptors by an associated phosphatase-kinase signaling complex. *Science* **285**, 93–96 (1999).
43. Day, M., Wokosin, D., Plotkin, J.L., Tian, X. & Surmeier, D.J. Differential excitability and modulation of striatal medium spiny neuron dendrites. *J. Neurosci.* **28**, 11603–11614 (2008).
44. Calabresi, P., Picconi, B., Tozzi, A. & Di Filippo, M. Dopamine-mediated regulation of corticostriatal synaptic plasticity. *Trends Neurosci.* **30**, 211–219 (2007).
45. Giuffrida, A. *et al.* Dopamine activation of endogenous cannabinoid signaling in dorsal striatum. *Nat. Neurosci.* **2**, 358–363 (1999).

ONLINE METHODS

Slice preparation and pharmacology. All animal handling was performed in accordance with guidelines approved by the Harvard Institutional Animal Care and Use Committee and federal guidelines. Recordings were made from green-fluorescing MSNs in striatal slices taken from male and female postnatal day 15–22 drd2-GFP mice[15,22] or Emx-Cre/drd2-GFP mice (see below) that were killed under isoflurane anesthesia. Coronal slices (300 μm thick) were cut in ice-cold external solution containing 110 mM choline, 25 mM $NaHCO_3$, 1.25 mM NaH_2PO_4, 2.5 mM KCl, 7 mM $MgCl_2$, 0.5 mM $CaCl_2$, 25 mM glucose, 11.6 mM sodium ascorbate and 3.1 mM sodium pyruvate, bubbled with 95% O_2 and 5% CO_2. Slices were then transferred to ACSF containing 127 mM NaCl, 25 mM $NaHCO_3$, 1.25 mM NaH_2PO_4, 2.5 mM KCl, 1 mM $MgCl_2$, 2 mM $CaCl_2$ and 25 mM glucose, bubbled with 95% O_2 and 5% CO_2. After an incubation period of 30–40 min at 34 °C, the slices were maintained at 22–25 °C until use. All experiments were conducted at 32 °C. In all experiments, the ACSF included 50 μM picrotoxin to block $GABA_{A/C}$ receptor–mediated inhibition and 10 μM scopolamine to block confounding actions of muscarinic acetylcholine receptors. For all glutamate uncaging experiments, 10 μM serine was included in the ACSF to reduce NMDAR desensitization. For some experiments, extracellular $MgCl_2$ was reduced to nominally 0 mM. Finally, in some experiments, one or more of the following drugs were added to the ACSF: 8 μM quinpirole, 10 μM CPP, 10 μM NBQX, 3 μM ifenprodil, 1 μM tetrodotoxin, 10 μM mibefradil, 0.1 μM SNX-482, 0.2 μM agatoxin IVA, 1 μM ω-conotoxin GVIA, 3 or 20 μM nimodipine, 0.1 μM apamin, 1 μM PKI(14-22), 10 μM H89, 0.2 μM CGS-21680 and 0.1 μM SCH-58261. All chemicals were from Tocris, with the exception of SNX-482, agatoxin IVA and ω-conotoxin GVIA which were from Peptides International.

Electrophysiology and imaging. Whole-cell recordings were obtained from D2R-expressing MSNs identified with video-infrared/differential interference contrast and GFP epifluorescence. Two-photon laser-scanning microscopy confirmed the presence of prominent dendritic spines. For current-clamp recordings, glass electrodes (2–3.5 MΩ) were filled with internal solution containing 135 mM $KMeSO_3$, 10 mM HEPES, 4 mM $MgCl_2$, 4 mM Na_2ATP, 0.4 mM NaGTP and 10 mM sodium creatine phosphate, adjusted to pH 7.3 with KOH. For voltage-clamp recordings, cesium was substituted for potassium to improve space clamp. For Ca^{2+}-imaging experiments, either 150 μM (**Figs. 5** and **8**), 600 μM (**Fig. 6**) or 300 μM (all other experiments) of the Ca^{2+}-sensitive indicator Fluo-5F and 10 μM Alexa Fluor-594 were added. As previous work has shown that membrane potential influences the Ca^{2+} sources activated during synaptic transmission[28], cells were held near −60 mV for current-clamp recordings to approximate the conditions of MSNs *in vivo*[46]. Voltage-clamp experiments were performed with a holding potential of −70 mV. All recordings were made using an Axopatch 200B amplifier, and data were filtered at 5 kHz and digitized at 10 kHz. For electrical activation of excitatory input fibers, brief (0.2 ms) current injections were applied to a small glass electrode (tip diameter, 2–4 μm) filled with ACSF and placed at the border between the striatum and the overlying white matter, 100–300 μm from the recorded cell.

Intracellular Ca^{2+} imaging and glutamate uncaging were accomplished with a custom microscope, as previously described[28]. The microscope was assembled using components manufactured by the Harvard Medical School Department of Neurobiology machine shop or Mike's Machine Company. Neurons were filled via the patch electrode for 10–15 min before imaging. Fluo-5F (green) and Alexa Fluor-594 (red) were excited using 840-nm light to monitor Ca^{2+} signals and spine morphology, respectively. To measure Ca^{2+} signals, we collected green and red fluorescence during 500-Hz line scans across a spine and a neighboring dendrite. Reference frame scans were taken between each acquisition to correct for small spatial drift of the preparation over time. Ca^{2+} signals were first quantified as increases in green fluorescence from baseline normalized to the average red

fluorescence ($\Delta G/R$). The elevated resting green fluorescence as a result of GFP expression slightly increased shot noise, but did not alter the Ca^{2+}-dependent signal magnitude or the linearity of the response. To allow greater generalization of the data across various microscope configurations, we expressed fluorescence changes as the percentage of the G/R ratio measured in saturating Ca^{2+} (G_{sat}/R) in a sealed recording pipette. To calculate G_{sat}/R, we imaged a 1:1 mixture of internal solution and 1 M $CaCl_2$ in the specimen plane under conditions identical to those used during recordings.

For two-photon laser uncaging experiments, MNI-glutamate was bath applied at 2.5 mM and glutamate uncaging was achieved using a 0.5-ms pulse of 725-nm light. To achieve standard uncaging power (which translates into a constant amount of glutamate uncaged on each trial), we used photobleaching of Alexa Fluo-594 in the spine of interest, as previously described[23]. Bleaching is a function of the laser power and provides a readout of power delivery that is independent of spine depth in the slice and electrophysiological responses.

Viral ChR2 expression and activation. To selectively express a conditional form of the light-activated membrane channel ChR2 (ref. 47) in corticostriatal afferents, we crossed drd2-GFP mice with mice expressing Cre recombinase under control of the *Emx1* promoter[48]. At postnatal day 12, the F1 offspring of these lines were injected intracranially into somatomotor cortex under isoflurane anesthesia with 1.0 μl of a recombinant adenoassociated virus (serotype 2/8, Harvard Gene Therapy Institute) containing a double *loxP*-flanked inverted construct coding for the fusion protein ChR2-mCherry under control of the *Ef1a* promoter[47]. Mice were killed 7–10 d post-injection for slice preparation as described above and exhibited strong labeling of descending cortical fibers that arborized throughout the dorsal striatum (**Fig. 1b**). To activate ChR2-positive fibers, we focused light from a 473-nm laser (Optoengine) on to the back aperture of the microscope objective, producing a wide-field exposure around the recorded MSN of 10–20 mW mm^{-2}. Brief (1–2 ms) pulses of light were delivered under control of the acquisition software.

Data acquisition and analysis. Imaging and physiology data were acquired using National Instruments data acquisition boards and custom software written in MATLAB (Mathworks)[49]. Off-line analysis was performed using custom routines written in MATLAB and Igor Pro (Wavemetrics). The amplitudes of all EPSPs and nonNMDAR-mediated EPSCs were calculated by averaging over a 3-ms window around the peak, whereas a 10-ms window was used to calculate amplitudes of NMDAR-mediated EPSCs. The amplitudes of triplet burst-evoked uEPSPs were calculated around the peak response following the third stimulus. For imaging experiments, measurements of $\Delta G/G_{sat}$ were calculated by taking the average of the signal over a 150-ms post-stimulus window.

In sections describing optical or uncaging responses measured from individual spines, the stated *n* indicates the number of spines analyzed. In sections describing electrically evoked synaptic responses, the stated *n* indicates the number of cells analyzed. All summary graphs and data are expressed as mean ± s.e.m. and comparisons were made using a two-tailed Student's *t* test unless otherwise stated. Differences were judged to be statistically significant for $P < 0.05$.

46. Mahon, S., Deniau, J.M. & Charpier, S. Relationship between EEG potentials and intracellular activity of striatal and cortico-striatal neurons: an *in vivo* study under different anesthetics. *Cereb. Cortex* **11**, 360–373 (2001).
47. Gradinaru, V., Mogri, M., Thompson, K.R., Henderson, J.M. & Deisseroth, K. Optical deconstruction of parkinsonian neural circuitry. *Science* **324**, 354–359 (2009).
48. Gorski, J.A. *et al.* Cortical excitatory neurons and glia, but not GABAergic neurons, are produced in the Emx1-expressing lineage. *J. Neurosci.* **22**, 6309–6314 (2002).
49. Pologruto, T.A., Sabatini, B.L. & Svoboda, K. ScanImage: flexible software for operating laser scanning microscopes. *Biomed. Eng. Online* **2**, 13 (2003).

Erratum: Competitive regulation of synaptic Ca^{2+} influx by D2 dopamine and A2A adenosine receptors

Michael J Higley & Bernardo L Sabatini
Nat. Neurosci.; doi:10.1038/nn.2592; corrected online 11 July 2010

The sizing of Figure 6 has been modified in the print, PDF and HTML versions of this article.